Separation Science and Technology
Publication details, including instructions for authors and subscription information:
http://www.informaworld.com/smpp/title~content=t713708471

Parametric Performance Analysis of an Electrostatic Wire-Cylinder Aerosol Separator in Laminar Flow Using a Numerical Modeling Approach

M. Alshehhi[a]; A. Shooshtari[a]; S. Dessiatoun[a]; M. Ohadi[b]; A. Goharzadeh[b]
[a] Department of Mechanical Engineering, University of Maryland at College Park, Maryland, USA [b] Department of Mechanical Engineering, Petroleum Institute, Abu Dhabi, UAE

Online publication date: 12 February 2010

To cite this Article Alshehhi, M. , Shooshtari, A. , Dessiatoun, S. , Ohadi, M. and Goharzadeh, A.(2010) 'Parametric Performance Analysis of an Electrostatic Wire-Cylinder Aerosol Separator in Laminar Flow Using a Numerical Modeling Approach', Separation Science and Technology, 45: 3, 299 — 309
To link to this Article: DOI: 10.1080/01496390903484859
URL: http://dx.doi.org/10.1080/01496390903484859

Separation Science and Technology, 45: 299–309, 2010

ISSN: 0149-6395 print/1520-5754 online
DOI: 10.1080/01496390903484859

Taylor & Francis
Taylor & Francis Group

Parametric Performance Analysis of an Electrostatic Wire-Cylinder Aerosol Separator in Laminar Flow Using a Numerical Modeling Approach

M. Alshehhi,[1] A. Shooshtari,[1] S. Dessiatoun,[1] M. Ohadi,[2] and A. Goharzadeh[2]
[1]*Department of Mechanical Engineering, University of Maryland at College Park, Maryland, USA*
[2]*Department of Mechanical Engineering, Petroleum Institute, Abu Dhabi, UAE*

A numerical methodology based on the Lagrangian approach is outlined to study the performance of a select class of electrostatic aerosol separators. This modeling method is used to perform a parametric study on the efficiency of a wire-cylinder separator in separation of water aerosols from air. The geometry consists of an 80 μm diameter wire placed in the centerline of a 20 mm diameter cylinder. The work focuses on the effect of applied voltage (in the range of 4 to 8 kV), flow velocity (in the range of 0.3 to 1.5 m/s), flow temperature (in the range of 280 K to 320 K), and separator length (in the range of 0.05 to 0.15 m) on charging of water aerosols and on separator collection efficiency in laminar flow. The aerosols size ranges between 0.01–10 μm. The results of the study show that applied voltage, flow rate, and separator length affect the separation efficiency significantly, while the effect of flow temperature seems negligible.

Keywords diffusion charging; electrohydrodynamics; electrostatic precipitator; field charging; numerical modeling; Rayleigh limit; separation; water aerosol

INTRODUCTION

The separation of suspended particles from gases has been one of the basic scientific and technical problems of the industrial era and this interest continues (1). Stricter environmental legislation and standards on emissions of fine particles have been motivating forces in development of more efficient separators. Different industrial applications, such as clean rooms for various operations, including micro and nano fabrication technologies, refrigeration and HVAC systems and many other applications, which require controlled aerosol concentrations in moving gaseous mediums to maintain system functionality and efficiency.

There is a variety of methods of separating aerosols from process streams using different principles, such as inertial separation as applied in cyclones, impaction and diffusion as used in coalescence force-based filters, electrostatic separation as applied in electrostatic precipitators, and so on (2). However, many industrial and conventional gas-liquid separators are limited in terms of separating fine aerosols from gas streams (3,4). For example, the conventional cyclone's efficiency falls dramatically when aerosol diameter size drops below 1 μm. This is because the cyclone's performance depends on the mass difference between the suspended liquid aerosols and the carrier gas, and this factor becomes insignificant in submicron aerosols. Although coalescence-based separators are more efficient, their performance decreases when the aerosol size is below 0.5 μm. In addition, this type of separator has a significant pressure drop and a high maintenance cost. Among these techniques, electrostatic precipitators (ESPs), which use electrostatic force to charge and collect particles, have shown many advantages. They have low pressure drop and maintenance cost and are highly efficient and reliable (5).

ESPs operate on the basic principle of gas-borne aerosols that are passed through a corona or charged field, where they receive an electric charge. Then the charged particles are deflected by the electric field and move across the gas stream from an emitter electrode to a collector electrode, where they are removed from gas stream. Two distinct mechanisms are active in charging the particles, diffusion charging and field charging. The aerosol's size plays an important role in determining the dominant charging mechanism. For a submicron aerosol, diffusion charging is more dominant, while field charging becomes the prevailing factor when the aerosol's diameter is in the micron range.

Figure 1 shows the diffusion charging in a charging and collecting particles process. The charging process starts when aerosols enter a region filled with randomly moving ions created by a high voltage difference between two electrodes. The ions move in random fluctuations due to the effect of Brownian motion. Since the kinetic energy due to Brownian motion is proportional to the temperature, then thermal motions of the ions cause them to diffuse through the gas and to collide with aerosols. Such ions

Received 13 April 2009; accepted 29 October 2009.
Address correspondence to M. Alshehhi, Department of Mechanical Engineering, University of Maryland at College Park, College Park, Maryland, USA. E-mail: alshehhi@umd.edu

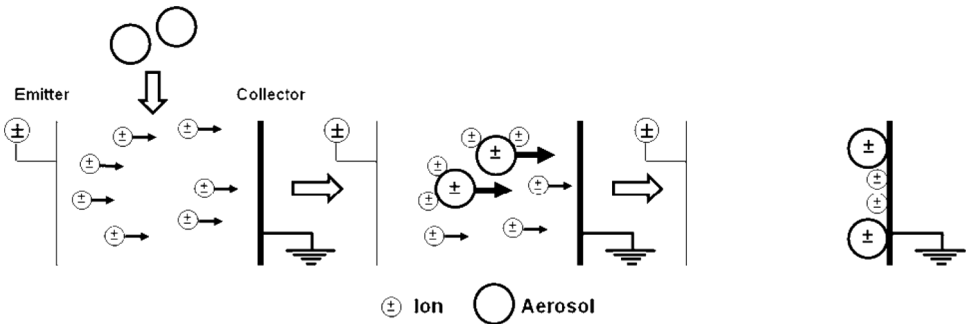

FIG. 1. Diffusion charging mechanism. Aerosols enter a region of moving ions, the aerosols absorb the charge after colliding with ions, the aerosols move to the opposite charge or ground surface.

will generally adhere to aerosols due to the attractive forces that exist between ions and droplets in general which are known to be as electrical-image forces. These forces come into play as the ions approach the aerosols. The accumulation of electric charge on an aerosol gives rise to a repelling field, which tends to prevent additional ions from reaching the aerosol. Thus, the rate of charging decreases as the charge accumulates on a particle and will ultimately proceed at a negligible rate. As the charge builds up, the aerosols move to the opposite charge or ground electrode. Since this type of charging process occurs through the random collisions between ions and particles, it is greatly affected by the charge density of ions. On the other hand, the electric field intensity and the aerosol material do not have a direct effect on the diffusion charging (6). Given that the random collision is based on Brownian motion, the temperature of the flow may also affect the charging process (see Eq. (11)).

In field charging, as depicted in Fig. 2, a liquid aerosol enters a region of traveling ions between electrodes. The presence of the aerosol disturbs the ions traveling along electrical field lines, so the ions strike the aerosol and transfer their charge to the aerosol's surface. After the aerosol gets charged, it moves to the opposite-charge or ground electrode. Unlike the diffusion charging process, this type of charging is affected greatly by the electric field.

Many researchers and scientists have tried to present the electrostatic effect on traveling particles using mathematical models. In 1824, M. Hohlfeld, a mathematics teacher in Leipzig, Germany, first described the precipitation of smoke particles by electricity (7). The first commercially successful process was developed in 1906 following experiments by F.G. Cottrell at the University of California, Berkeley (8). In 1926, Deutsch made the first attempt to derive a theoretical equation for the particle charging process, but his attempt failed because he did not recognize the difference between diffusion and field charging (9). A few years later, Arendt and Kallmann came up with the first theoretical expression for the diffusion charging that gave the rate of particle charging, assuming that the particle had already taken an appreciable charge (10). For field charging, Rohmann and Pauthenier, working individually, derived a theoretical expression for field charging (11,12).

Numerical simulation of the separation process in ESPs involves modeling the electrohydrodynamic (EHD) flow, due to interaction of the electric field and space charge within the fluid flow, as well as the particle movement. To model the effect of all of these phenomena, one should solve the Maxwell equation for the electrostatic field and space charge coupled with both particle dynamics and Navier-Stokes equations. In terms of particle movement, both Eulerian and Lagrangian approaches have been

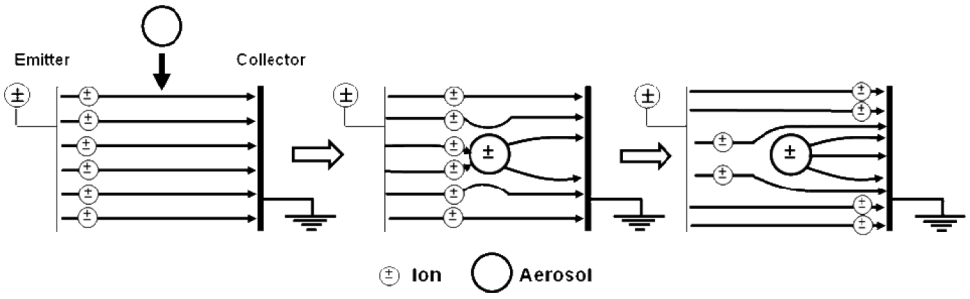

FIG. 2. Field charging mechanism. An aerosol enters a region of traveling ions along field lines because of a gradient in electric field. The aerosol's size is big enough to be stroked by ions and absorb the charge, and the aerosol moves to opposite charge.

widely used to predict particle dispersion in an ESP. The Eulerian method is based on solving the continuity equation of particles to obtain particle concentration distribution, while in the Lagrangian method the momentum equation for each particle is solved to obtain its trajectory. The performance characterization of ESPs depends on the solution of this coupled problem, which can be obtained with a varying degree of accuracy using different models characterized by different degrees of complexity and computational cost.

Parker in his book presented some cases that highlighted the efficiency of electrostatic precipitators with different flow conditions (13). He used the theoretical migration velocity of solid particles (such as dust or smoke) that was obtained by Riehle to calculate the separation efficiency (14). When he compared the theoretical and experimental outcomes, he found that the efficiency for the experimental work was much higher than the theoretical one.

Goo and Lee developed a numerical scheme to estimate the collection efficiency of particles in the wire-plate ESP (15). Some of the physical phenomena they considered were corona-field, turbulent EHD flow-field, in situ particle charging, and turbulent motion of particles. They used the Lagrangian particle-tracking method coupled with the Monte-Carlo method for simulating the stochastic nature of turbulence to overcome the deficiencies of the Eulerian method. The analytical code was used to analyze an experimental work done earlier by Kihm (16). The calculated efficiency was lower than the experimental one due to many factors such as the difficulty in estimating the exact charging properties of the particles used in the experiment and the inlet conditions of the flow and the particles.

Talaie et al. developed a numerical model based on the Eulerian approach to predict the performance of a double-stage electrostatic precipitator (17). In their work, the effect of polydisperse particle loading was directly included in the velocity distribution, electrical field distribution, and particle concentration. Also, the change in gas eddy diffusivity was considered in their model. Their results confirmed the significant effect of particle size distribution on ESP performance.

Sugita et al. investigated the behavior of water aerosols in an air-water separator (18). The study used theoretical analysis to investigate the motion of a water aerosol under electrostatic forces and the theoretical length of separator needed to collect the aerosols. The mean diameter of the water aerosols they used was 30 μm. They were able to obtain an analytical equation for the minimum length needed to collect the aerosols.

Soldati later on developed a two-dimensional Eulerian, advection-diffusion type model for particle transport with distributed parameters (19). A cost function for a model ESP was defined, and the influence of a number of design parameters on cost and collection efficiency was examined. The results showed that the most cost-effective way to increase the collection efficiency of a wire-plate ESP is to decrease the wire-to-wire distance.

Then Talaei came up with a two-dimensional mathematical model for the performance of wire-duct, single-stage electrostatic precipitators (20). The main objective of his model was to study the effect of inlet particle concentration and applied voltage on corona sheath thickness. He used the Lagrangian approach to predict the movements of particles. He found that increasing particle concentration participates in quenching corona sheath thickness.

Lei et al. performed a numerical study to investigate the behavior of charged particles in electrostatic precipitators for turbulent flow (21). They used the Eulerian approach to simulate the electrostatic fields and the Langragian approach for in situ particle charging and tracking. They found that for particles smaller than 0.1 μm, the flow turbulence had a very significant effect on their movements, but the difference of charge among particles was not obvious. On the other hand, particles larger than 10 μm were not influenced by the flow turbulence in their movememnt, but they reached the saturation charge quickly. For particles lying in between, the effect was not obvious.

In this work, the performance of a wire-cylinder ESP has been studied numerically. A mathematical model has been developed based on a modified Lagrangian approach to simulate the ESP performance on separating water aerosols from an air flow when applied voltage, ESP geometry, and flow conditions have been changed. Also, the accumulated charge on droplets has been obtained and shown that their breakup due to the charge accumulation is unlikley.

MATHEMATICAL MODEL

To develop the mathematical model, the following simplifying assumptions were made:

- All the particles are spherical.
- The accumulated charge on each particle does not affect the local electric field.
- Due to low concentration, there is no interaction among the particles.
- The temperature of the particles and fluid are the same.
- The fluid flow field is not affected by the motion of the particles.

Next, we consider an aerosol subject to electric and fluid flow fields. The trajectory can be determined from the momentum balance applied to this particle.

$$\frac{d\mathbf{u}_p}{dt} = F_D(\mathbf{u} - \mathbf{u}_p) + \frac{\mathbf{g}(\rho_p - \rho)}{\rho_p} + \mathbf{F}_e \qquad (1)$$

The Stokes drag term is given as

$$F_D = \frac{C_D \mathrm{Re}}{24} \frac{18\mu}{\rho_p d_p^2} \tag{2}$$

where the drag coefficient (C_D) for spherical particles is calculated by using the correlations developed by Morsi and Alexander for different ranges of Reynolds numbers (22). The Reynolds number (Re) can be defined as

$$\mathrm{Re} = \frac{\rho d_p |\mathbf{u}_p - \mathbf{u}|}{\mu} \tag{3}$$

For submicron particles, drag force acting on the particles is independent of the Reynolds number. Stokes's law assumes that the relative velocity of the gas at the surface of a droplet is zero. Since this assumption is not accurate for submicron aerosols, the Cunningham correction factor (C_c) must be included in the calculation of the drag force (23).

$$F_D = \frac{1}{C_c} \frac{18\mu}{\rho_p d_p^2} \tag{4}$$

$$C_c = 1 + \frac{2\lambda}{d_p}\left(1.257 + 0.4e^{\frac{-1.1 d_p}{2\lambda}}\right) \tag{5}$$

The velocity of fluid ($\mathbf{u}$) can be obtained from continuity and the Navier-Stokes equations.

$$\nabla \cdot \mathbf{u} = 0 \tag{6}$$

$$\rho(\mathbf{u} \cdot \nabla \mathbf{u}) = -\nabla P + \mu \nabla^2 \mathbf{u} + \mathbf{F}_{EHD} \tag{7}$$

where $\mathbf{F}_{EHD}$ is the electrohydrodynamic body force applied to the aerosol carrier fluid and is given as

$$\mathbf{F}_{EHD} = \rho_i \mathbf{E} \tag{8}$$

where ρ_i and $\mathbf{E}$ are the ionic charge density and the electric field, respectively.

The last term in Eq. (1) represents the electrostatic body force exerted on a charged aerosol, given as

$$\mathbf{F}_e = \frac{q_p \mathbf{E}}{1/6\pi d_p^3 \rho_p} \tag{9}$$

To calculate this body force, the local electric field in vicinity of aerosol particle ($\mathbf{E}$) and the charge accumulated on the particle (q_p) must be determined. The total particle charge is the summation of diffusion charging and field charging.

$$q_p = q_{diff} + q_{fld} \tag{10}$$

Assuming that every ion that strikes an aerosol droplet due to Brownian motion is captured, the amount of accumulated diffusion charge on a given spherical particle is given by

$$q_{diff} = \frac{d_p kT}{2K_E e} \ln\left(1 + \frac{\pi K_E d_p \overline{C}_i e \rho_i t}{2kT}\right) \tag{11}$$

where $\overline{C}_i$ is the mean thermal speed of the ions, t is time interval and T is fluid temperature. As can be seen, the diffusion charging mechanism is not directly affected by the electric field intensity, and as time passes, the rate of charging gradually slows down.

The amount of charge acquired by an aerosol particle due to the field charging process is

$$q_{fld} = \left(\frac{3\varepsilon_p}{\varepsilon_p + 2}\right)\left(\frac{\mathbf{E} d_p^2}{4K_E}\right)\left(\frac{\pi K_E Z_i \rho_i t}{1 + \pi K_E Z_i \rho_i t}\right) \tag{12}$$

where ε_p is the relative permittivity of the particle and Z_i is the mobility of ions. Aerosols charged by the field charging mechanism reach saturation charge status as time passes, wherein they repel any additional ions from reaching the aerosols. The amount of charge at saturation state is

$$q_{fld,sat} = \left(\frac{3\varepsilon_p}{\varepsilon_p + 2}\right)\left(\frac{\mathbf{E} d_p^2}{4K_E}\right) \tag{13}$$

In order to determine the ion charge density (ρ_i) and electric field intensity ($\mathbf{E}$), the Poisson's and conservation of charge equations must be solved:

$$\nabla^2 \phi = -\frac{\rho_i}{\varepsilon} \tag{14}$$

$$\frac{\partial \rho_i}{\partial t} + \nabla \cdot \mathbf{J} = 0 \tag{15}$$

where ϕ is the potential field, ε is the permittivity of fluid, and $\mathbf{J}$ is the current density. The relation between potential and electric fields is given by

$$\mathbf{E} = -\nabla \phi \tag{16}$$

The current density is the summation of ionic mobility, conduction, and convection components, respectively, given as

$$\mathbf{J} = \rho_i Z_i \mathbf{E} + \sigma_i \mathbf{E} + \rho_i \mathbf{u} \tag{17}$$

Since the electrical conductivity of gases is negligible, and the velocity of fluid ($\mathbf{u}$) is much less than ion velocity ($Z_i \mathbf{E}$), then the last two terms in Eq. (17) can be dropped out. Therefore,

$$\mathbf{J} = \rho_i Z_i \mathbf{E} \tag{18}$$

The total electrical current passing from the charged electrode (emitter) to the ground electrode (collector) is given by

$$I = \int_{A_0} \mathbf{J} \cdot \mathbf{dA} \tag{19}$$

where A_0 is any closed area that encloses the emitter or collector electrodes.

The boundary conditions must also be specified to be able to solve the set of governing equations and determine the trajectory of every aerosol particle entering the computational domain. The boundary condition for Eq. (1) at the injection point is given by

$$\mathbf{u}_p = \mathbf{u}_{inj} \tag{20}$$

where $\mathbf{u}_{inj}$ is the velocity of the particle which must be specified.

The boundary conditions for Eq. (7) depend on the given geometry and are straightforward. For example, on walls, the no-slip condition is imposed. For Eq. (14) following boundary conditions are enforced.

$$\begin{cases} \phi = \phi_e & \text{on the charged electrode (emitter) surface} \\ \phi = 0 & \text{on the ground electrode (collector) surface} \\ \frac{d\phi}{dn} = 0 & \text{on all other surfaces} \end{cases} \tag{21}$$

where ϕ_e is the applied voltage to the emitter electrode and n is local unit vector normal to the surface. Here it is assumed that, except the emitter and collector electrodes, all other surfaces are perfectly insulated.

The boundary conditions for charge density calculated from Eq. (15) are more involved, and various approaches have been suggested. In the current work, it is assumed that

$$\begin{cases} \rho_i = \rho_{i,e} & \text{on the charged electrode surface} \\ \frac{d\rho_i}{dn} = 0 & \text{on the ground electrode surface and all other surfaces} \end{cases} \tag{22}$$

where $\rho_{i,e}$ is the charge density on the emitter surface and its value is assumed to be known. If the current-voltage characteristic (CVC) of the separator is known, then $\rho_{i,e}$ can be set such that the calculated current from Eq. (19) matches the experimental current for a given voltage.

When dealing with charging liquid droplets, the issue of droplets breaking up due to the charge accumulation on their surfaces arises (24). The reason for this behavior is that the mutual repulsion force of the electric charges at the droplet's surface exceeds the confining force of the surface tension. At this point, the droplet will be broken into smaller drops in order to create more surface area for the charge. The maximum amount of charge that a liquid particle can have is called the Rayleigh limit and depends on particle's type and size. This limit generally cannot be reached except in the case of small droplets. The limiting charge is given by

$$q_R = \sqrt{\frac{2\pi\gamma d_p^3}{k_E}} \tag{23}$$

The performance of the electrostatic separation is characterized based on its efficiency defined as

$$\eta = 1 - \frac{\text{No. of Escaped Particles}}{\text{No. of Injected Particles}} \tag{24}$$

NUMERICAL METHOD

The commercial CFD code Fluent (version 6.2, Lebanon, NH) was used to solve the governing equations. Since the Fluent code does not provide a built-in solver for potential and charge conservation equations (i.e., Eqs. (14) and (15)), a user-defined program determining the charge density and the electric fields as well as the aerosols charging was written and incorporated with the main source code (25). The electrostatic force influence on aerosol droplets was modeled through an applied body force as described in Eq. (1). The major steps of numerical solution are as follows:

- Solve for the electric and ion charge density fields using Poisson's and charge conservation equations.
- Solve for the flow field using Navier-Stokes and continuity equations.
- Track particles using momentum equations and determine temporal charge accumulation on particles as they travel.

This numerical method can be applied to various ESP geometries to study their performances. Since this method is based on the Lagrangian approach, the polydisperse aerosol particles injection can easily be incorporated.

WIRE-CYLINDER AEROSOL SEPARATOR

The numerical method was used to perform a parametric study on classic wire-cylinder geometry. This is a simple geometry that conveniently represents many industrial applications. Moreover, from a modeling perspective, the advantage of this geometry is the availability of analytical solutions for electric field governing equations (i.e., Eqs. (14) and (15)). Therefore, the numerical results of these equations can be compared against the analytical solutions (see Appendix (A) for analytical solutions). The numerical results of aerosols tracking can be used to investigate the efficiency of this class of separators for

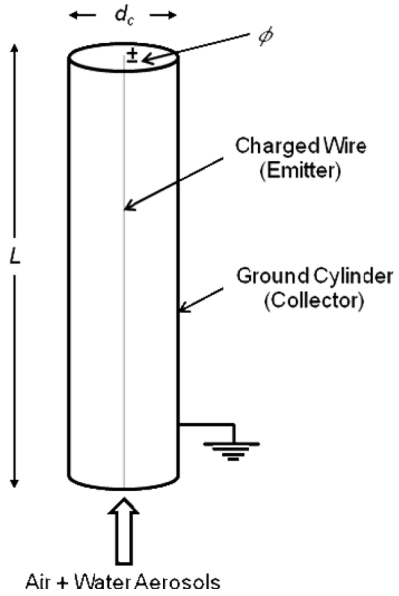

FIG. 3. Wire-cylinder schematic where L: separator length, d_c: cylinder diameter (grounded), ϕ: applied electric potential at the wire (charged).

separation of fine droplets. The schematic configuration of the wire-cylinder separator is shown in Fig. 3.

In this modeling the particles were water aerosol droplets carried with the air stream. The modeling input parameters listed in Tables 1 and 2 summarize the selected range of parameters used in this study. For each modeling case, only one parameter changed at a time.

Due to symmetry, only half of the cylindrical tube was considered as the computational domain. Also, since the electric force exerted on the airflow was axisymmetric, no recirculation was created, and air fluid flow was not affected by EHD interaction. Therefore, $\mathbf{F}_{EHD}$ in Eq. (7) was not considered.

The computational domain was descritized to 487520 computational cells using Tri-Pave meshing scheme in each cross-section as well as uniform meshing in axial direction. To capture the high intensity electric field, a high concentration of cells was created in the vicinity of the wire electrode.

TABLE 1
Modeling input variables

Cylinder diameter (m)	$d_c = 0.02$
Wire diameter (m)	$d_w = 0.00008$
Fluid density (kg/m^3)	$\rho = 1.18$
Fluid viscosity (kg/(m · s))	$\mu = 1.86 \times 10^{-5}$
Fluid permitivity (F/m)	$\varepsilon = 8.854 \times 10^{-12}$
Aerosol relative permitivity	$\varepsilon_p = 80$
Ions mean thermal speed (m/s)	$\overline{C}_i = 240$
Ions mobility (m^2/(V · s))	$Z_i = 1.5 \times 10^{-4}$

TABLE 2
Modeling varied parameters

Wire electric potential (kV)	$\phi = 4, 5, 6, 7, 8$
Average air flow inlet velocity (m/s)	$\mathbf{u} = 0.3, 0.6, 0.9, 1.2, 1.5$
Air flow temperature (K)	$T = 280, 300, 320$
Separator length (m)	$L = 0.05, 0.075, 0.1, 0.125, 0.15$

For the fluid flow boundary condition, the fully developed parabolic velocity profile was imposed at the tube inlet such that the average inlet velocity was equal to those values given in Table 2. For the electric field, the wire electric potential was set based on values given in Table 2, and the tube wall was always grounded. The charge density on the wire electrode was set using the analytical solutions of Eqs. (14) and (15) presented in Appendix (A). First, the initial electric field at the wire (E_0) was calculated using Peek's formula, Eq. (A6). Then the analytical solution of Poisson's equation for cylindrical coordinates, Eqs. (A2), (A4), and (A5) were used to calculate the charge density on the wire. Both applied potential and charge density on the wire were fed to the numerical solution.

The particles were injected using uniform surface distribution injection. Preliminary tests of the model showed that the number of injected particles affects the separation efficiency significantly if it is lower than 200 particles. To minimize any error and to insure the efficiency independence on the particle number, 500 equally distant particles were injected in each study. The particles were assumed to be at a halt once they were injected, and they gradually accelerated along the airflow due to the drag force. The particles that were deflected by the electric field force and which collided with the tube wall were totally collected, and no reflection existed.

RESULTS

The first step in generating results was to obtain the current vs. voltage curve (CVC) to characterize the separator performance and to calculate the power consumption. Figure 4 shows the CVC for the given separator geometry. The minimum voltage to sustain a corona discharge for the conditions studied here was 4 kV, which is in agreement with the corona onset voltage given by Eq. (A8).

First, the numerical model solution for potential field and charge density had to be verified against the analytical solution. Figures 5 and 6 show comparisons between both numerical and analytical results for the electric potential and charge density distribution along the radial distance, respectively. As seen there, a favorable agreement between

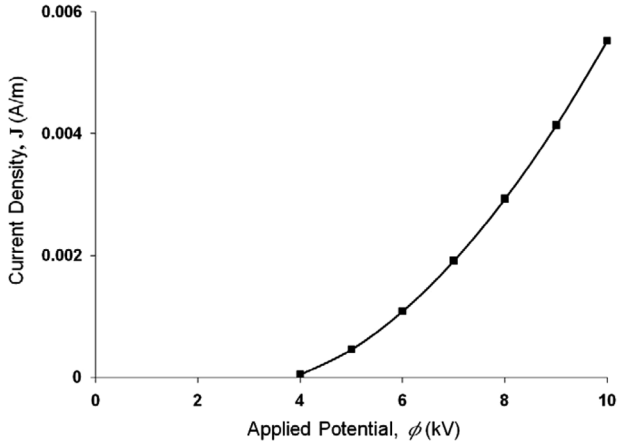

FIG. 4. Current-voltage characteristics curve for the wire-cylinder separator at $T = 300\,\mathrm{K}$.

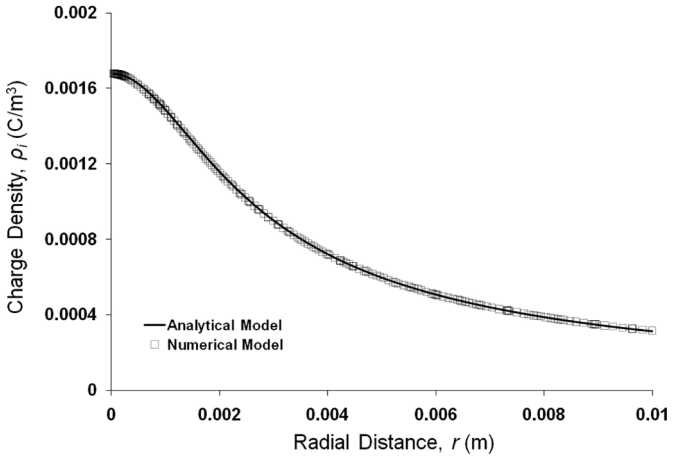

FIG. 6. Comparison in charge density between numerical and analytical models at $\phi = 6.0\,\mathrm{kV}$, $\mathrm{u} = 1.0\,\mathrm{m/s}$, $T = 300\,\mathrm{K}$ and $L = 0.15\,\mathrm{m}$.

the results was obtained. The results show that the charge density decreases more than four-fold as one moves from the emitter to collector surfaces.

Particle size plays an important role in how the particle is charged. Figure 7 shows the average of the number of charges accumulated on injected particles as they travel inside the separator by each of the two different charging mechanisms as well as the combined effect. It can be seen from the figure that particles of less than 0.5 μm are charged mainly through diffusion charging, where particles of size greater than 0.5 μm are predominantly charged through field charging.

In order to ensure the water aerosol droplets maintained their integrity and did not break into parts as they moved inside the high electric field, the number of accumulated charges had to be checked against the Rayleigh limit. Figure 8 shows the maximum number of accumulated charges over all the injected aerosol droplets. The difference ratio between the Rayleigh limit and the maximum accumulated charge on a particle ranged between 65–150. Therefore, the limit was not reached in this study.

The first case in the parametric study investigated the effect of applied electric potential on separation efficiency defined by Eq. (24). Figure 9 shows five cases where a potential increase improved separation efficiency. The reason for this is that increasing the electric potential leads to enhancement of the electric field intensity and an increase of charge density, which both enhance the charging process.

The efficiency generally starts decreasing as the aerosol diameter size gets bigger than 0.01 μm, and then it starts increasing once diameter size passes 0.5 μm. The reason for this behavior is that the total charging is the summation

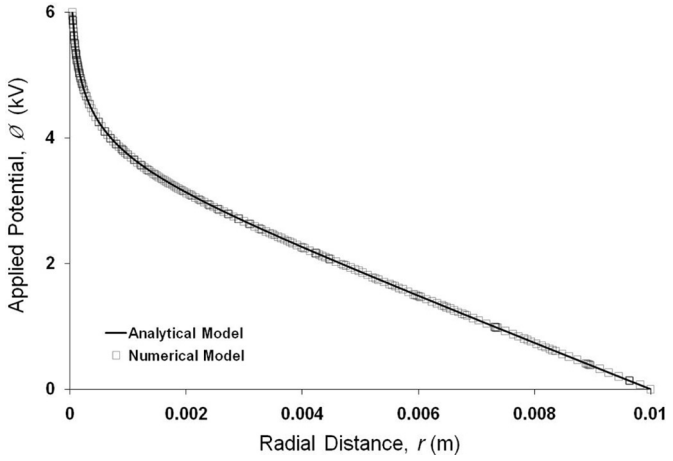

FIG. 5. Comparison in electric potential field between numerical and analytical models at $\phi = 6.0\,\mathrm{kV}$, $\mathrm{u} = 1.0\,\mathrm{m/s}$, $T = 300\,\mathrm{K}$ and $L = 0.15\,\mathrm{m}$.

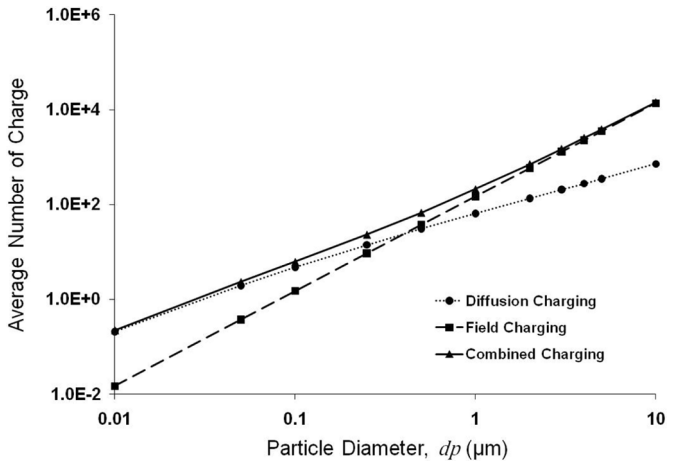

FIG. 7. Average number of charge accumulated on a particle due diffusion charging, field charging or diffusion and field charging. The varied parameters are $\phi = 4.0\,\mathrm{kV}$, $\mathrm{u} = 1.0\,\mathrm{m/s}$, $T = 300\,\mathrm{K}$ and $L = 0.15\,\mathrm{m}$.

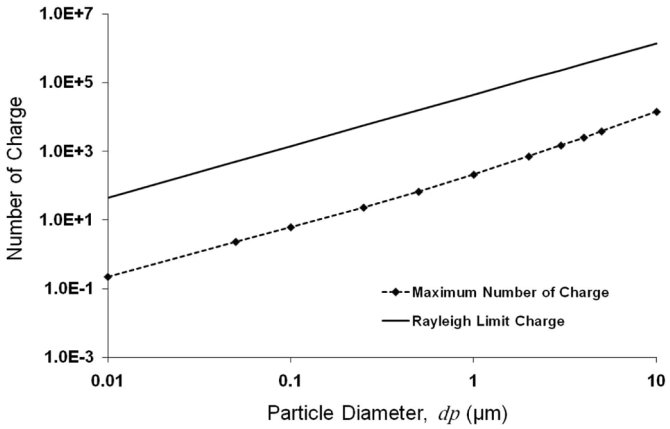

FIG. 8. Comparison between Rayleigh limit and the maximum number of charges accumulated on a particle due to diffusion and field charging. The varied parameters are $\phi = 4.0\,\text{kV}$, $u = 1.0\,\text{m/s}$, $T = 300\,\text{K}$ and $L = 0.15\,\text{m}$.

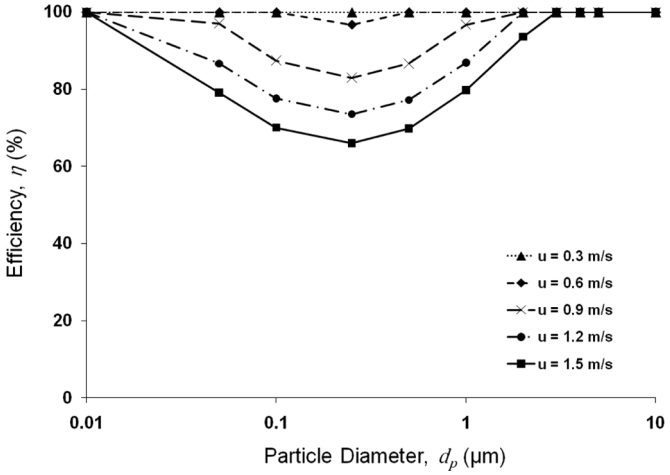

FIG. 10. Flow rate effect on separation efficiency for five cases with the following input parameters: $\phi = 6.0\,\text{kV}$, $T = 300\,\text{K}$ and $L = 0.15\,\text{m}$.

of diffusion and field charging. The diffusion charging mechanism is the more dominant factor on small particles, while the field charging is more dominant on larger particles. However, the combined effects are less effective when the particle size is in-between. Looking at case (5) where the voltage is 8 kV, 100% efficiency was reached at all different aerosols diameters. The power consumption in this case was about 2.4 W.

The next case addressed the effect of flow rate on charging and collecting water aerosols. As expected, increasing the flow rate lowered the efficiency because of the shorter resident time available for the aerosols to receive charge, to travel to the collector electrode, and get trapped, as Fig. 10 shows. For example, in case number (1), where the velocity was 0.3 m/s, the efficiency was 100% at all different diameter sizes, while for velocity 1.5 m/s the minimum efficiency decreased to 66% at diameter size 0.25 μm.

The third case investigated the effect of flow temperature on the separation efficiency. As mentioned earlier, in diffusion charging ions move due to Brownian motion. Based on Eq. (11), the flow temperature can affect this charging mechanism, the primary method of charging of small particles (i.e., <0.5 μm). The result of our study, presented in Fig. 11, shows that over the investigated range of temperatures, the temperature influence is minimum and is only on small particles. Overall, the effect of temperature on the separation efficiency can be disregarded without any substantial error. The temperature change is considered on the thermophysical properties of gas and particles such as density and viscosity.

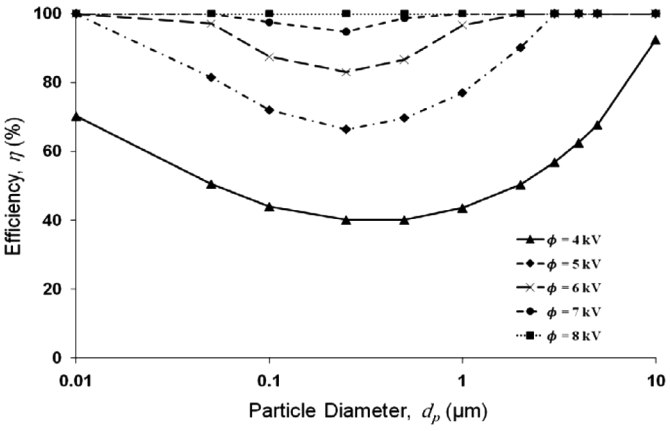

FIG. 9. Electric potential field effect on separation efficiency for five cases with the following input parameters: $u = 0.9\,\text{m/s}$, $T = 300\,\text{K}$ and $L = 0.15\,\text{m}$.

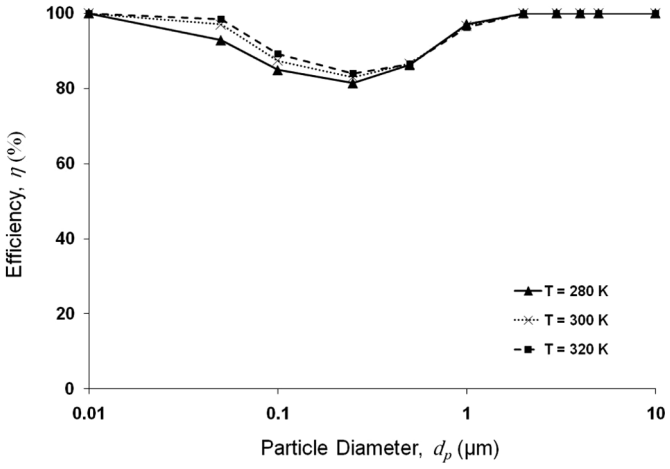

FIG. 11. Flow temperature effect on separation efficiency for three cases with the following input parameters: $\phi = 6.0\,\text{kV}$, $u = 0.9\,\text{m/s}$ and $L = 0.15\,\text{m}$.

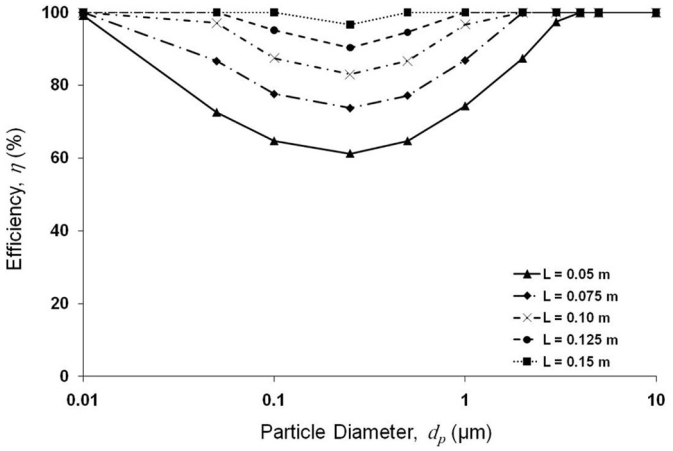

FIG. 12. Separator length effect on separation efficiency for five cases with the following input parameters: $\phi = 6.0\,\text{kV}$, $\text{u} = 0.9\,\text{m/s}$ and $T = 300\,\text{K}$.

The last case investigated the effect of the separator length on separation performance. Figure 12 shows that as the length increased, so did the separation efficiency. Increasing the length means increasing the aerosol residence time as well as the collection area, which eventually enhances the performance of the separator. As seen there, the minimum efficiency varied from 61% for 0.05 m separator to 100% for 0.15 m separator.

MESH STUDY

A mesh study was conducted to investigate the independency of numerical model results with the number of computational cells. The study used the same meshing scheme, Tri-Pave, but with finer and coarser computational grids. Figure 13 shows a comparison between three cases that had the same input parameters with different cell numbers, where (a) was with decreased cell numbers, (b) was the standard case and (c) was with increased cell numbers. The averaged difference between cases (a) and (b) was about 0.5% where the difference between cases (b) and (c) was about 0.8%. Therefore, for the parametric study in this paper it can be concluded that within ±1% the results are independent of the cell number. Thus, the computational cells number can be increased to improve the accuracy.

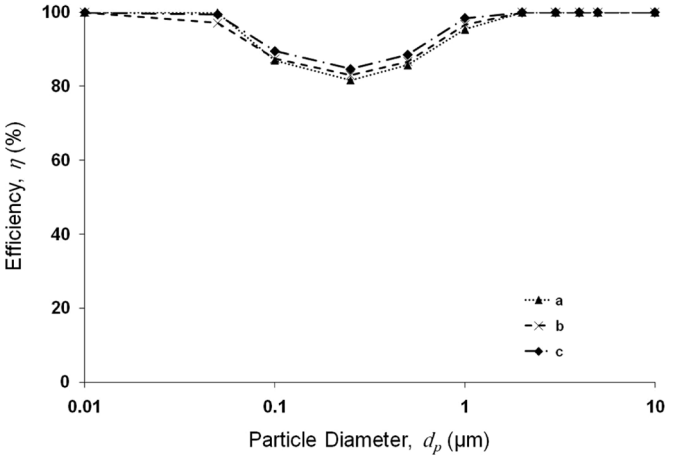

FIG. 13. Mesh study comparison between three cases that have the same parameters such as: $\phi = 6\,\text{kV}$, $\text{u} = 0.9\,\text{m/s}$, $T = 300\,\text{K}$, and $L = 0.10\,\text{m}$ with different computational cell numbers, as $\text{a} = 94655$ cells, $\text{b} = 487520$ cells and $\text{c} = 753840$ cells.

CONCLUSIONS

A numerical methodology based on the Lagrangian approach was outlined to study the performance of electrostatic aerosol separators in laminar flow. A parametric study on the performance of electrostatic separator was performed, and the influences of applied potential, fluid velocity, temperature, and separator geometry were investigated. Based on the results obtained, increasing the applied voltage and separator length directly increases the separation efficiency. On the other hand, the efficiency decreases as the flow velocity increases. The effect of flow temperature on the performance of the separator was found to be insubstantial. Electrostatic separation can be considered an energy-efficient mechanism at low air velocities. Numerically, it can achieve 100% efficiency with reasonable power consumption, 2.4 W for a voltage of 8 kV and wire length of 0.1 m in the present study. Based on collective findings of this study the electrostatic separation appears to be a promising solution to the separation area of water aerosols from air flow.

NOMENCLATURE

$\mathbf{A}$	area (m^2)
A_0	any closed area that encloses emitter or collector electrodes (m^2)
C_1	constant
C_2	constant
C_c	Cunningham correction factor
C_D	drag coefficient
$\overline{C}_i$	ion mean thermal speed (m/s)
d_c	cylinder diameter (m)
d_p	particle diameter (m)
d_w	wire diameter (m)
$\mathbf{E}$	electric field strength (V/m)
E_0	initial electric field strength at emitter (V/m)
e	electron charge (1.6×10^{-19} C)
F_D	drag term (s^{-1})
$\mathbf{F}_e$	electrostatic body force (N/m^2)
$\mathbf{F}_{EHD}$	electrohydrodynamic body force (N/m^2)
$\mathbf{g}$	acceleration due gravity (m/s^2)
$\mathbf{J}$	current density (A/m^3)
k	Boltzmann constant ($1.3806503 \times 10^{-23}\,\text{m}^2/(\text{kg} \cdot \text{s}^2 \cdot \text{K})$)

k_E	proportionality constant ($9.0 \times 10^9\ \mathrm{N \cdot m^2/C^2}$)
L	separator length (m)
n	local unit vector normal to the surface
P	actual fluid pressure (mm of mercury column)
P_0	normal atmospheric pressure (mm of mercury column)
q_{diff}	charge on a particle due to diffusion charging (C)
q_{fld}	charge on a particle due to field charging (C)
$q_{fld,sat}$	saturation charge on a particle due to field charging (C)
q_p	charge on a particle due to diffusion and field charging (C)
q_R	limiting charge on a particle due to Rayleigh limit (C)
r	radial distance in x-direction (m)
Re	Reynolds number
T	actual fluid temperature (K)
T_0	absolute ambient temperature (K)
t	resident time (s)
$\mathbf{u}$	fluid velocity (m/s)
$\mathbf{u}_{inj}$	injection point velocity (m/s)
$\mathbf{u_p}$	particle velocity (m/s)
Z_i	ion mobility ($\mathrm{m^2/(V \cdot s)}$)
ϕ	electric potential (V)
ϕ_0	corona onset voltage (V)
ϕ_e	electric potential at emitter (V)
μ	fluid viscosity ($\mathrm{N \cdot s/m^2}$)
γ	surface tension of a particle (N/m)
δ	relative density
ε	permittivity of a vacuum ($8.85 \times 10^{-12}\ \mathrm{C^2/(N \cdot m^2)}$)
ε_p	relative permittivity of a particle
η	separation efficiency (%)
λ	molecular mean free path (m)
ρ	fluid density ($\mathrm{kg/m^3}$)
ρ_i	charge density of space ($\mathrm{C/m^3}$)
$\rho_{i,e}$	charge density at emitter ($\mathrm{C/m^3}$)
ρ_p	particle density ($\mathrm{kg/m^3}$)
σ_i	electric conductivity (S/m)

REFERENCES

1. White, H.J. (1963) *Industrial Electrostatic Precipitation*, 1st Ed.; Addison-Wesley Publishing Company Inc.: Portland, Oregon.
2. Bürkholz, A. (1989) *Droplet Separation*; Weinheim: VCH Verlagsgesellschaft.
3. Scharge, D.; Shoemaker, J.; McQuillen, J. (1998) Passive two-phase fluid separation. *AIAA 36th Aerospace Sciences Meeting & Exhibit. AIAA-98-0731*, Reno, Nevada.
4. TeGrotenhuis, W.; Stenkamp, V. (2001) Normal gravity testing of a microchannel phase separator for in-situ resource utilization. Battelle Memorial Institute, Richland, VA.
5. Mizuno, A. (2000) Electrostatic precipitation. *Dielectrics and Electrical Insulation*, 7 (5): 615.
6. Hohlfeld, M. (1824) Das niederschlagen des rauches durch elektricitat. *Archiv. fur die gesammte Naturlehre.*, 2: 205.
7. Hoppel, W.; Frick, G. (1986) Ion-aerosol attachment coefficients and the steady-state charge distribution on aerosols in a bipolar environment. *J. Aerosol Science and Technology*, 5: 1.
8. Cottrell, F.G. (1911) The electrical precipitation of suspended particles. *J. Industrial and Engineering Chemistry*, 8 (3): 542.
9. Deutsch, W. (1922) Bewegung und ladung der elektricitatstrager im zylinder kondensator. *Annalen der Physik.*, 68: 335.
10. Arendt, P.; Kallmann, H. (1926) The mechanism of charging mist particles. *Z. Phys.*, 35: 421.
11. Rohmann, H. (1923) Messung der grosse von schwebeteilchen. *Z. Phys.*, 17: 253.
12. Pauthenier, M.; Moreau-Hanot, M. (1932) La charge des particulates spheriques dans un champ ionise. *Journal de Physique et le Radium.*, 3: 590.
13. Parker, K. (1997) *Applied Electrostatic Precipitation*, 1st Ed.; Chapman & Hall: London, U.K.
14. Riehle, C. (1929) Bewegung und abscheidung von partikeln im elektrofilter. Doctorate Thesis, University of Karlsruhe.
15. Goo, J.; Lee, J. (1997) Stochastic simulation of particle charging and collection characteristics for a wire-plate electrostatic precipitator of short length. *J. Aerosol Science*, 28 (5): 875.
16. Kihm, K. (1987) Effects of nonuniformities on particle transport in electrostatic precipitators. Ph.D. Thesis, Standford University, Stanford.
17. Talaie, M.; Fathikaljahi, J.; Taheri, M.; Bahri, P. (2001) Mathematical modeling of double-stage electrostatic precipitators based on a modified eulerian approach. *Aerosol Science and Technology*, 34 (6): 512.
18. Sugita, H.; Nakazawa, T.; Jiao-Long, L.; Tao, X. (2003) Study on the behavior of droplet in air-water separator. *J. Japan Institution of Marine Engineering*, 38 (2): 72.
19. Soldati, A. (2003) Cost-efficiency analysis of a model wire-plate electrostatic precipitator via DNS based eulerian particle transport approach. *Aerosol Science and Technology*, 37 (2): 171.
20. Talaie, M. (2005) Mathematical modeling of wire-duct single-stage electrostatic precipitators. *J. Hazardous Materials*, 124 (1–3): 44.
21. Lei, H.; Wang, L.-Z.; Wu, Z.-N. (2008) EHD turbulent flow and Monte-Carlo simulation for particle charging and tracing in a wire-plate electrostatic precipitator. *J. Electrostatics*, 66 (3–4): 130.
22. Morsi, S.; Alexander, A. (1972) An investigation of particle trajectories in two-phase flow systems. *J. Fluid Mechanics*, 55 (2): 193.
23. Qunis, H.; Ahmadi, G.; McLaughlin, J. (1991) Bownian diffusion of submicrometer particles in the viscous sublayer. *J. Colloid and Interface Science*, 143 (1): 266.
24. Hinds, W. (1999) *Aerosol Technology: Properties, Behavior and Measurement of Airborne Particles*, 2nd Ed.; John Willy & Sons Inc.: Los Angeles, California.
25. Shooshtari, A. (2004) Experimental and computational analysis of an electrohydrodynamic mesopump for spot cooling applications. Doctoral Thesis Dissertation, University of Maryland, Mechanical Engineering, College Park.
26. Feng, J. (1999) An analysis of corona currents between two concentric cylindrical electrodes. *J. Electrostatics*, 4: 37.
27. Peek, F. (1929) *Dielectric Phenomena in High Voltage Engineering*, 1st Ed.; McGraw-Hill: New York.

APPENDIX

All the equations listed in this section are for the specific case of wire-cylinder geometry. The Poisson's equation, Eq. (14), and current density, Eq. (18), in cylindrical coordinate can be written as:

$$\frac{1}{r}\frac{d}{dr}r\frac{d\phi}{dr} = -\frac{\rho_i}{\varepsilon} \tag{A1}$$

$$\mathbf{J} = 2\pi r \rho_i Z_i \mathbf{E} \tag{A2}$$

By combining Eqs. (16), (A1) and (A2), the resultant equation is given as

$$\frac{1}{r}\frac{d}{dr}\left(r\frac{d\phi}{dr}\right)^2 = -\frac{\mathbf{J}}{2\pi Z_i \varepsilon} \tag{A3}$$

where two solutions exist for equation (A3) (26).

For $C_1 \geq 0$, the soution is

$$\phi = -\sqrt{\left(\frac{\mathbf{J}}{2\pi Z_i \varepsilon}\right) r^2 + C_1} + \sqrt{C_1} \ln\left(\frac{\sqrt{\left(\frac{\mathbf{J}}{2\pi Z_i \varepsilon}\right) r^2 + C_1} + \sqrt{C_1}}{r}\right) + C_2 \tag{A4}$$

For $C_2 < 0$, the solution is

$$\phi = -\sqrt{\left(\frac{\mathbf{J}}{2\pi Z_i \varepsilon}\right) r^2 + C_1} + \sqrt{-C_1} \arctan\left(\frac{\sqrt{\left(\frac{\mathbf{J}}{2\pi Z_i \varepsilon}\right) r^2 + C_1}}{\sqrt{-C_1}}\right) + C_2 \tag{A5}$$

To calulate the CVC, the threshold field strength can be determined semiempirically using Peek's formula (27).

$$E_0 = 30\delta + 9\sqrt{\frac{2\delta}{d_w}} \tag{A6}$$

where the unit of E_0 is (kV/cm) and δ is identified as the relative density and can be calculated as

$$\delta = \frac{T_0}{T}\frac{P}{P_0} \tag{A7}$$

Equation (A6) can be used with one of the soutions, either Equations (A4) or (A5) to find the resultant current for a given voltage. The given voltage should be higher than the corona onset voltage (ϕ_0) which can identified as

$$\phi_0 = \frac{d_w}{2} E_0 \log\frac{d_c}{d_w} \tag{A8}$$

The charge density adjacent to the emitter electrode plays an important role in shaping current-voltage relation as it reduces local field strength. This will cause the calculated current to have a maximum limit at a given applied voltage (27).